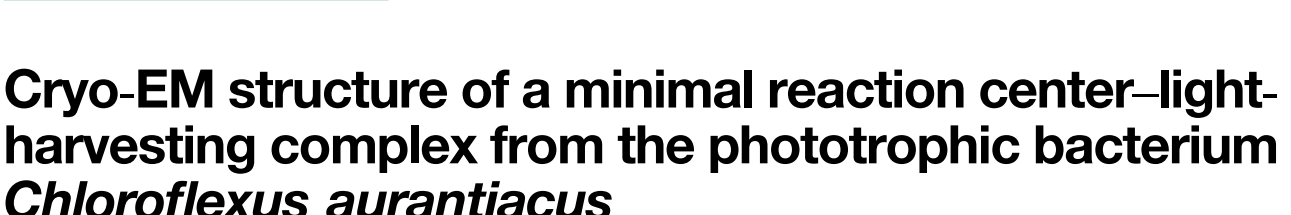
Check for







Guoqiang Huang<sup>1,2†</sup>, Shishang Dong<sup>3†</sup>, Lin Ma<sup>3†</sup>, Lin Li<sup>3</sup>, Jinxin Ju<sup>3</sup>, Mei-Jiao Wang<sup>4</sup>, Jian-Ping Zhang<sup>4</sup>, Sen-Fang Sui<sup>1,5</sup>, and Xiaochun Qin<sup>3</sup>

- 1. State Key Laboratory of Membrane Biology, Beijing Advanced Innovation Center for Structural Biology, School of Life Sciences, Tsinghua University, Beijing 100084, China
- 2. Multiscale Research Institute of Complex Systems, Fudan University, Shanghai 200433, China
- 3. School of Biological Science and Technology, University of Jinan, Jinan 250022, China
- 4. School of Chemistry and Life Resources, Renmin University of China, Beijing 100872, China
- 5. School of Life Sciences, Southern University of Science and Technology, Shenzhen 518055, China

\*Correspondences: Sen-Fang Sui (suisf@mail.tsinghua.edu.cn); Xiaochun Qin (bio\_qinxc@ujn.edu.cn; Dr. Qin is fully responsible for the distributions of all materials associated with this article)





**Guoqiang Huang** 

Xiaochun Qin

## **ABSTRACT**

Photosynthetic organisms have developed various light-harvesting antenna systems to capture light and transfer energy to reaction centers (RCs). Simultaneous utilization of the integral membrane light-harvesting antenna (LH complex) and the extrinsic antenna (chlorosomes) makes the phototrophic bacterium *Chloroflexus* (*Cfx.*) *aurantiacus* an ideal model for studying filamentous anoxygenic

phototrophs (FAPs). Here, we determined the structure of a minimal RC-LH photocomplex from Cfx. aurantiacus J-10-fl (CaRC-LH) at 3.05-Å resolution. The CaRC-LH binds only to seven LH subunits, which form a crescent-shaped antenna surrounding the movable menaguinone-10 (Q<sub>B</sub>) binding site of CaRC. In this complex with minimal LH units, an extra antenna is required to ensure sufficient light-gathering, providing a clear explanation for the presence of chlorosomes in Cfx. aurantiacus. More importantly, the semicircle of the antenna represents a novel RC-LH assembly pattern. Our structure provides a basis for understanding the existence of chlorosomes in Cfx. aurantiacus and the possible assembly pattern of RC-LH.

Keywords: *Chloroflexus aurantiacus*, chlorosomes, electron transfer, photosynthesis, RC–LH

Huang, G., Dong, S., Ma, L., Li, L., Ju, J., Wang, M. J., Zhang, J. P., Sui, S. F., and Qin, X. (2025). Cryo-EM structure of a minimal reaction center–light-harvesting complex from the phototrophic bacterium *Chloroflexus aurantiacus*. J. Integr. Plant Biol. **00**: 1–12.

# INTRODUCTION

Photosynthesis involves the most important photobiochemical reactions on Earth. Light energy is captured by intra- or extra-membrane light-harvesting (LH) antenna before being transferred to membrane-embedded reaction centers (RCs), where charge separation initiates electron transfer (ET) (Qian et al., 2018). Reaction centers in phototrophs can be categorized as Type I or Type II. Type I RCs use iron-sulfur clusters as electron acceptors, while Type II

RCs utilize quinones (Hager-Braun et al., 1995). All anoxygenic phototrophic bacteria employ a single type of RC to drive ET for photosynthesis, with green sulfur bacteria (phylum Chlorobi) (Chen et al., 2020), Heliobacterium modesticaldum (phylum Firmicutes) (Gisriel et al., 2017), Chloracidobacterium thermophilum (phylum Acidobacteria) (Dong et al., 2022), and Candidatus Chlorohelix allophototropha (phylum Chloroflexi) (Tsuji et al., 2024) using Type I RCs and purple bacteria (phylum Proteobacteria) (Yu et al., 2018), Gemmatimonas phototrophica (G. phototrophica, phylum

<sup>&</sup>lt;sup>†</sup>These authors contributed equally to this work.

Gemmatimonadetes) (Qian et al., 2022), Candidatus Eremiobacterota (candidate phylum Eremiobacterota) (Ward et al., 2019), and most members of the phylum Chloroflexi using Type II RCs (Tsuji et al., 2024).

Members of the phototrophic group in the phylum Chloroflexi are also called filamentous anoxygenic phototrophs (FAPs). Currently, phylum Chloroflexi contains at least three families (Chloroflexaceae, Oscillochloridaceae, and Roseiflexaceae) (Rosenberg, 2014) that share the following features. First, all existing FAPs except Candidatus Chlorohelix allophototropha utilize Type II RCs to drive photochemistry. Second, FAPs with Type II RCs possess only one kind of membrane-embedded light-harvesting antenna (called LH), which is distinct from the two kinds of antenna used in purple bacteria, namely, the core light-harvesting complex 1 (LH1) and the accessory light-harvesting complex 2 (LH2) (Blankenship, 2014). At the same time, different FAPs tend to have different photosynthetic apparatuses. For instance, Chloroflexus (Cfx.) aurantiacus (Chloroflexaceae) (Tang et al., 2011) and Oscillochloris trichoides (Oscillochloridaceae) (Taisova et al., 2002) possess chlorosomes, the ellipsoid supramolecular antenna complexes located on the cytoplasmic side (Hanada et al., 2002). Species equipped with chlorosomes capture light and transfer energy to special pairs of RCs even under extremely weak light conditions (Pedersen et al., 2010; Saer and Blankenship, 2017). By contrast, Roseiflexus (Rfl.) castenholzii from the Roseiflexaceae lacks chlorosomes. Previous research has suggested that the ancestors of the phylum Chloroflexi had chlorosomes, but lost them during evolution (Xin et al., 2018), meaning that Cfx. aurantiacus may have a more primitive photosynthetic apparatus than Rfl. castenholzii.

In recent years, structures of the RC-LH1 complexes from G. phototrophica (Qian et al., 2022) and various purple bacteria have been determined at near-atomic resolution (Liu et al., 2023; Swainsbury et al., 2023), such as those of Blastochloris (Blc.) viridis (Qian et al., 2018), Thermochromatium (Tch.) tepidum (Yu et al., 2018), Thiorhodovibrio strain 970 (Tani et al., 2020), Rhodopseudomonas (Rps.) palustris (Swainsbury et al., 2021), Rhodobacter (Rba.) veldkampii (Bracun et al., 2021), Rhodospirillum (Rsp.) rubrum (Tani et al., 2021a), Rhodopila (Rpi.) globiformis (Tani et al., 2022a), Rba. sphaeroides (Qian et al., 2021a, 2021b; Tani et al., 2021b; Cao et al., 2022), Allochromatium (Alc.) tepidum (Tani et al., 2022b), and Rba. capsulatus (Bracun et al., 2023; Tani et al., 2023). These structures revealed the cofactor-binding architecture of many subunits, including L, M, H, and LH1 with or without cytochrome (Cyt) c subunits, as well as interactions between these subunits. Rfl. castenholzii RC-LH (RcRC-LH) complexes in native and carotenoid-depleted states have also been determined (Xin et al., 2018, 2023; Qi et al., 2023). RcRC (PDB ID: 8J5P), composed of L, M, X, Y, Z, and Cyt c subunits, is surrounded by an open elliptical LH ring comprising 15 LH  $\alpha\beta$ -heterodimers. RcRC lacks the H subunit typically found in the RC of purple bacteria, but contains the newly identified transmembrane (TM) domain-containing protein Z located at the corresponding position to the H subunit (Qi et al., 2023; Xin et al., 2023). In addition, two additional subunits with single TM domains (protein X and Y) are also present in the RcRC-LH complex (Xin et al., 2018, 2023; Qi et al., 2023). These structural details provide a glimpse into the diversity of the photosynthetic apparatus. However, all of the above structures, whether from G. phototrophica, purple bacteria, or Rfl. castenholzii, are for Type II RCs from anoxygenic phototrophic organisms that lack chlorosomes; a structure for a Type II RC from anoxygenic phototrophs that binds chlorosomes has not previously been reported.

Here, we report a 3D cryo-electron microscopy (cryo-EM) structure for an RC-LH photocomplex from the chlorosomescontaining strain Cfx. aurantiacus J-10-fl (Chloroflexaceae) at 3.05 Å resolution. Our structure reveals a minimal RC-LH complex, with only seven LH subunits asymmetrically arranged on one side of the CaRC. This structural analysis uncovers the detailed organization and cofactor arrangement within the complex, offering new insight into the structural diversity of Type II RC-antenna complexes. Furthermore, it provides important clues into the evolutionary changes that have occurred in the supramolecular organization of RC-LHs due to changes in light environments.

# **RESULTS**

### Structure of the CaRC-LH

We isolated CaRC-LH complexes from Cfx. aurantiacus J-10-fl cultures grown photoheterotrophically under anoxic conditions by sucrose density gradient centrifugation (Figure S1A) (Pierson and Castenholz, 1974; Pierson and Thornber, 1983). We then subjected the purified CaRC-LH complex to cryo-EM single-particle analysis (Figure S2). Briefly, we captured 5,757 micrographs using a Titan Krios microscope, resulting in 589,587 particles auto-picked by Topaz. Through multiple rounds of 2D classification and ab initio reconstruction, 36,181 particles were selected to yield a final reconstruction with an overall resolution of 3.05 Å (Table S1). The CaRC-LH complex, with dimensions of approximately 110 × 100 × 85 Å (Figure 1A) and total molecular mass of ~250 kDa, is composed of L, M, and Cyt c subunits for the central CaRC, seven  $\alpha/\beta$ -heterodimer subunits for the surrounding LH, one previously undescribed TM helix protein (which we dubbed N), and 47 cofactors (Figure 1B). All unambiguous cryo-EM maps are presented in Figure S3.

The central CaRC contains 11 TM helices, with five located in the L subunit, five in the M subunit, and one in the Cyt c subunit (Figure 2A), closely resembling the architecture of RcRC (Xin et al., 2018). The L/M heterodimer carries two bacteriochlorophyll a molecules (BChls a) that form a special pair (P<sub>870</sub>), one BChl a (B<sub>A</sub>), three bacteriopheophytin a (BPheo a) molecules ( $\Phi_B$ ,  $H_A$ , and  $H_B$ ), two menaguinone-10 molecules (QA and QB), and one manganese ion (Mn). All of these cofactors are arranged into two branches, termed the A  $(P_{870}-B_A-H_A-Q_A)$  and B  $(P_{870}-\Phi_B-H_B-Q_B)$  branches (Figure 2A).

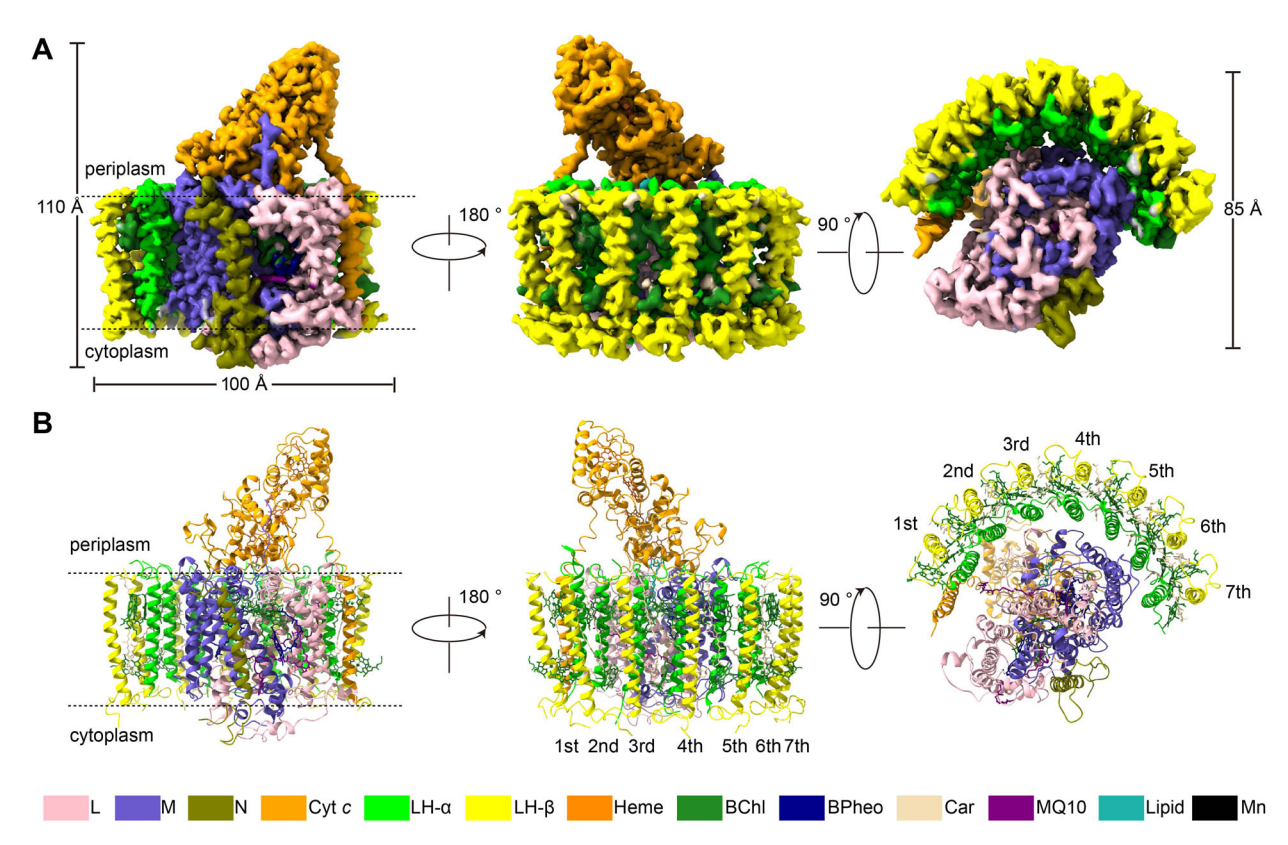


Figure 1. Cryo-EM structure of the CaRC-LH complex (A) Three different surface views of the cryo-EM density map of the CaRC-LH complex. (B) Architectural model of the CaRC-LH complex in three different

views corresponding to (A). The overall dimensions of the CaRC-LH complex are shown in (A). The light-harvesting (LH) subunits are numbered in (B). The color scheme is given at the bottom of the figure as follows: L, pink; M, slate blue; N, olive green; Cyt c, light orange; LH-α, lime green; LH-β, yellow; heme, dark orange; BChl, forest green; BPheo, dark blue; Car, tan; MQ10, purple; lipid, sea green; Mn, black.

Notably, this arrangement deviates from perfect symmetry: in the A branch,  $B_A$  is a BChl a, whereas in the B branch,  $\Phi_B$ is a BPheo a. This subtle asymmetry is likely to be a critical feature that enables functional specialization during ET. Such a structural arrangement mirrors the pattern observed in RcRC (Xin et al., 2018) and aligns with prior findings (Jun et al., 2020). P<sub>870</sub> is separated by an interplane distance of 8.3 Å, wherein the magnesium (Mg<sup>2+</sup>) ions are coordinated by the His213 residue in L and the His192 residue in M. The accessory BA molecule is coordinated by the conserved His193 residue in L (Figure 2B). Compared with the B<sub>B</sub> (a BChl a) in purple bacterial RCs (Qian et al., 2018; Yu et al., 2018; Tani et al., 2020, 2021a, 2021b, 2022a, 2022b, 2023; Bracun et al., 2021; Swainsbury et al., 2021; Cao et al., 2022; Bracun et al., 2023), the accessory  $\Phi_B$  is a BPheo in the CaRC and is immobilized by a non-ligand Leu172 residue in M instead of the conserved His residue that is present in most purple bacteria at this position (Figure 2B). Based on our density map and previous reports (Kirmaier et al., 1986; Qi et al., 2023), we did not position the metal ion iron (Fe) between two menaquinone sites as reported by Xin et al. (2023) in the RcRC-LH complex. Instead, we tentatively placed Mn there. The Mn ion is coordinated by five conserved residues (His267 in L, His230 in L, His209 in

M, His256 in M, and Glu224 in M) from the L/M heterodimer and transfers electrons from Q<sub>A</sub> to Q<sub>B</sub> (Figure 2B).

We compared the cryo-EM structures of the CaRC and RcRC (Xin et al., 2023), purified from Cfx. aurantiacus and Rfl. castenholzii cells, respectively, both grown under the same light intensity (~2,000 lx). We noticed that, in the CaRC, eight of nine distances between the adjacent cofactors along the A branch to Q<sub>B</sub> were shorter compared with those in the RcRC (Figure S4), meaning that the CaRC is likely to have a faster ET than the RcRC. However, the returned value of the lowest excited state of P<sub>870</sub> (P<sub>870</sub>\*) lifetime was reported to be ~7 ps, and the lifetime of the charge-separated state P<sub>870</sub><sup>+</sup>H<sub>A</sub><sup>-</sup> lifetime in the CaRC was reported as ~300 ps, which is somewhat longer than the ~3 and ~200 ps published values for the RcRC (Collins et al., 2011; Becker et al., 1991; Xin et al., 2007), contradicting our hypothesis. This discrepancy suggests that the ET process is affected not only by the distances between the ET cofactors, but also by the protein environments surrounding the ET cofactors.

In our cryo-EM structure, the electron donor Cyt c subunit is tightly inserted into the membrane by its N-terminal TM helix, nearly parallel to the inner  $\alpha$  apoprotein of LH, leaving its heme-binding domain to protrude into the periplasmic space. Thus, the four hemes (Heme 1, Heme 2, Heme 3, and

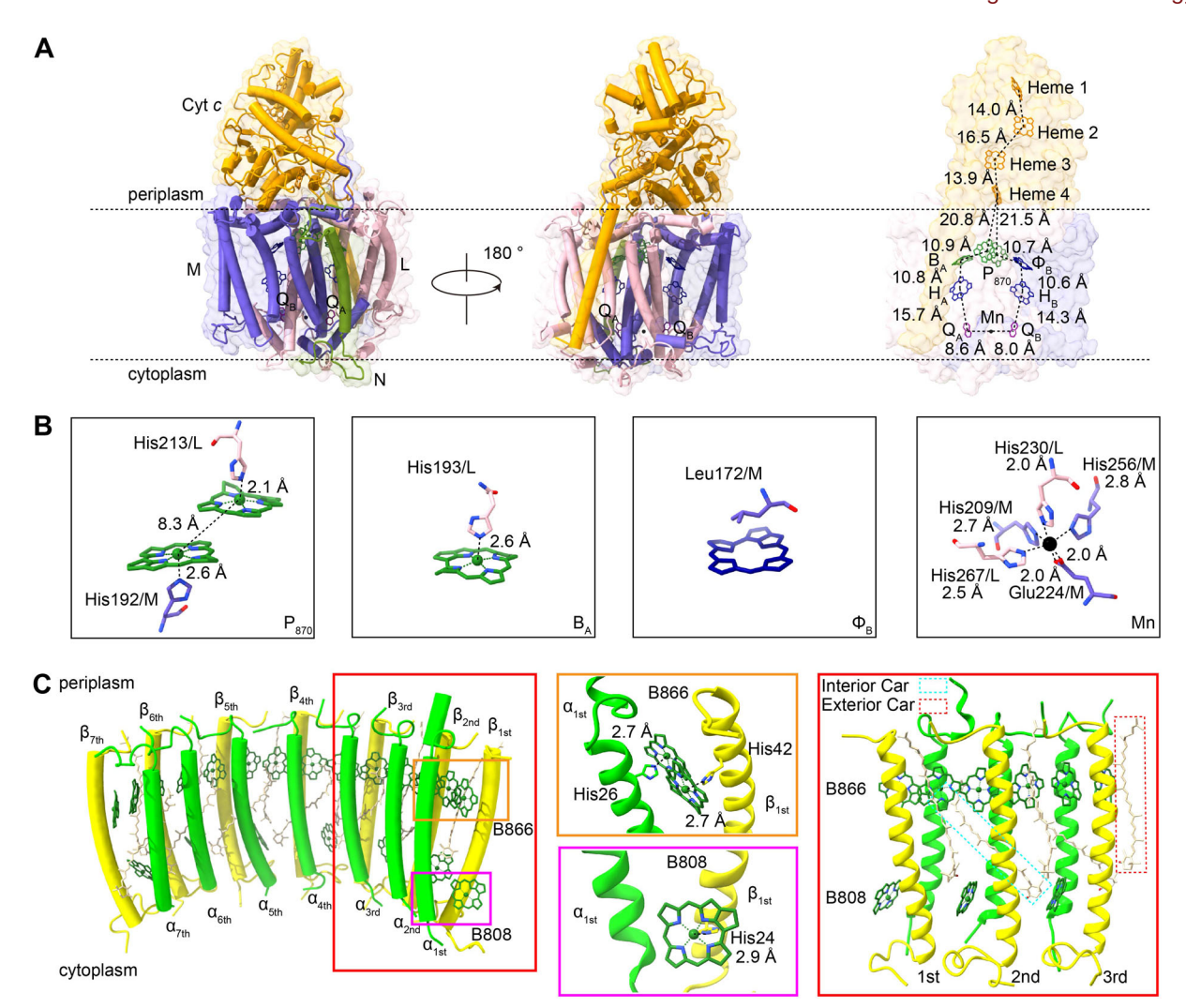


Figure 2. Distribution of subunits and cofactors in the CaRC–LH complex
(A) The subunits and cofactors in CaRC. (B) Coordinating environments for the cofactors in the electron transfer (ET) chain. (C) Subunits and pigments in the light-harvesting (LH) antenna. The center-to-center distances between the cofactors (black dotted lines) are given in Å. For clarity, the tails of BChls, BPheo, and MQ10 are all omitted.

Heme 4) are arranged in Cyt c with sufficiently short distances between adjacent hemes to efficiently donate electrons to the special pair (Figure 2A). Based on our high-quality density map, we identified a previously undescribed TM helix protein we named protein N (Figures S3, S5A); In our structure, protein N occupies a similar position to protein Z in RcRC-LH found in Cfx. aurantiacus (Qi et al., 2023; Xin et al., 2023) and creates a relatively enclosed pocket for QA binding (Figures 1A, 2A, S5B). Indeed, this density does not match that of the homologous sequence (Sequence ID: NWG19514.1) for protein Z in RcRC-LH. Further structural superposition showed that the location of protein N is also similar to that of the N-terminal helix of the H subunit in all known RC complexes from purple bacteria (Figure S5C) (Qian et al., 2018; Yu et al., 2018; Tani et al., 2020, 2021a, 2021b, 2022a; Bracun et al., 2021; Swainsbury et al., 2021; 2022b; Bracun et al., 2023). This finding strongly indicates that protein N is likely to play a role similar to that of the H subunit in assembling the RC complex, explaining why the H subunit is absent in FAPs. Importantly, we did not find a density consistent with the single TM protein Y (also known as protein I) observed in RcRC–LH in our structure (Qi et al., 2023; Xin et al., 2023). This absence leads to a noticeable increase in the size of the gap between the crescent-shaped LH antenna and the CaRC.

Surprisingly, the CaRC–LH complex contains only seven LH subunits, which is the smallest number of antennae reported among anoxygenic phototrophs with Type II RCs. These subunits are arranged in a unique crescent-shaped architecture on one side of the CaRC, while the other side is fully exposed to the surrounding membrane region (Figures 1B, 2C). Recently, the RC–LH1 photocomplexes of *Rba. capsulatus* contains 10 (small) (Tani et al., 2023) and 15 (large) LH1  $\alpha\beta$ -heterodimers (Bracun et al., 2023) have been reported, respectively. Although both the small form of *Rba. capsulatus* RC–LH1 complex and the CaRC–LH complex

#### Journal of Integrative Plant Biology

Structure of RC with seven LHs from Chloroflexus aurantiacus

have the semicircular antenna, but their arrangements are completely different. In *Rba. capsulatus*, the 10 LH1 subunits assemble around the RC near the  $Q_A$  side, while the seven LH subunits assemble close to the  $Q_B$  side of the CaRC in *Cfx. aurantiacus* (Figure S6). Compared with RcRC–LH, CaRC–LH lacks the 8–15th LH subunits, making the  $Q_A$  exposed to the membrane region. Therefore the  $Q_A$  in CaRC is in a completely different environment from that in RcRC, where the  $Q_A$  is surrounded by LH subunits.

In detail, every LH subunit of CaRC–LH is assembled by the TM helices from an inner  $\alpha$  apoprotein and an outer  $\beta$  apoprotein, with their N and C termini directed toward the cytoplasmic and periplasmic sides, respectively (Figure 2C). Sequence alignment between the LH- $\alpha$  and LH- $\beta$  apoproteins from *Cfx. aurantiacus* and their counterparts from *Rfl. Castenholzii*, *G. phototrophica*, and several purple bacteria showed high sequence similarity (Figure S7), reflecting billions of years of evolutionary conservation.

According to our density map, we unambiguously identified one BChl a molecule (B808) located near the cytoplasmic side and one pair of BChl a molecules (B866) near the periplasmic side from the αβ-heterodimeric LH, which is remarkably consistent with the previous report that CaRC-LH exhibits two absorption peaks at 808 and 866 nm (Vasmel et al., 1986; Xin et al., 2005). The porphyrin ring of B808 is inserted between neighboring  $\beta$  apoproteins in the outer layer of LH and coordinated by His24 in β. Two B866 pigments are ligands of His26 in  $\alpha$  and His42 in  $\beta$ , distributed parallel to each other between the inner and outer layers of the components of one pair of αβ-heterodimers and almost perpendicular to the porphyrin ring of B808. The shortest edge-toedge distances between adjacent B866 porphyrin rings (ranging from 2.9 to 3.9 Å) are generally shorter than those in RcRC (Figure S8). This arrangement may lead to the formation of stronger  $\pi$ – $\pi$  interactions among LH subunits in the CaRC-LH complex compared with the RcRC-LH complex (Zheng et al., 2021). Moreover, the shortest edge-to-edge distances of the porphyrin rings between adjacent B808 rings (ranging from 14.7 to 16.3 Å) and from B866 to B808 (ranging from 14.3 to 15.4 Å) in individual LH subunits in the CaRC-LH complex are also mostly shorter than those in the RcRC-LH complex (Figure S8). All of these unique arrangements of B808 and B866 allowed seven LH subunits to form a stable crescent-shaped antenna in the CaRC-LH complex.

Within the CaRC–LH complex, we observed additional weak or discontinuous densities in the LH subunits, positioned similarly to keto- $\gamma$ -carotene in the RcRC–LH complex from *Rfl. castenholzii* (Xin et al., 2023). However, previous HPLC analysis identified  $\gamma$ -carotene as the primary carotenoid in the B808–866 complex of *Cfx. aurantiacus* J-10-fl (Xin et al., 2005). Based on this, we tentatively assigned 13  $\gamma$ -carotene molecules to these densities. Seven interior  $\gamma$ -carotene molecules are inserted diagonally into the membrane, with one end positioned near the B866/ $\alpha$  of LH $_n$  and the other end close to the B808 of LH $_{n+2}$ . The remaining six  $\gamma$ -carotene molecules are located in the exterior of the LH, almost parallel to the adjacent

 $\beta$  apoproteins. All of these  $\gamma\text{-carotene}$  molecules transfer energy to the BChls and provide a photoprotective function against damaging excited states.

#### Interactions between subunits

Within each LH  $\alpha\beta$ -heterodimer, between adjacent LH subunits, and between the LH and the CaRC, we observed a multitude of hydrophobic interactions and other types of interactions. Collectively, these interactions ensure tight associations of the central CaRC, protein N, and the crescent-shaped LH subunits within the minimal CaRC-LH complex.

Within LH subunits, multiple hydrogen bond and salt bridge interactions are present between the  $\alpha$  and  $\beta$  apoproteins in different  $\alpha\beta$ -heterodimers (Figure 3A). In LH<sub>1st</sub>, LH<sub>2nd</sub>, LH<sub>3rd</sub>, LH<sub>6th</sub>, and LH<sub>7th</sub>, all Arg8 residues in  $\alpha$  form salt bridges with their respective Asp20 residues in  $\beta$  in the TM region near the cytoplasmic side. Notably, on the periplasmic side, we observed an additional salt bridge between Glu34 in  $\alpha$  and Lys49 in  $\beta$  in LH<sub>3rd</sub> in our structure. In LH<sub>4th</sub>, only two salt bridges form on the cytoplasmic side: one between Arg4 in  $\alpha$  and Asp4 in  $\beta$  and another between Arg4 in  $\alpha$  and Asp5 in  $\beta$ . However, we detected no salt bridge between the  $\alpha$  and  $\beta$  apoproteins in LH<sub>5th</sub>, but only a few hydrogen bonds.

We detected no salt bridge between adjacent LH subunits, but all LH subunits form hydrogen bonds with their neighbors, except LH<sub>6th</sub> and LH<sub>7th</sub> (Figure 3A). More precisely, there are two hydrogen-bonding interactions between  $LH_{1st}$  and  $LH_{2nd}.$  The first interaction is Arg8 in  $\alpha_{1st}\!\!-\!\!Ser5$  in  $\alpha_{2nd}$ , and the second is Gln19 in  $\beta_{1st}$ -Ser5 in  $\alpha_{2nd}$  on the cytoplasmic side. In contrast, there is only one hydrogen bond present on the periplasmic side between LH<sub>2nd</sub> and  $LH_{3rd}$ ,  $LH_{3rd}$  and  $LH_{4th}$ , and  $LH_{5th}$  and  $LH_{6th}$ . These interactions are Trp48 in  $\beta_{2nd}$ -Pro53 in  $\beta_{3rd}$ , Asn40 in  $\alpha_{3rd}$ -Glu34 in  $\alpha_{4\text{th}}$ , and Ser39 in  $\alpha_{5\text{th}}$ -Glu34 in  $\alpha_{6\text{th}}$ . Moreover, we observed several hydrogen bonds between LH<sub>4th</sub> and LH<sub>5th</sub>, including Gln19 in  $\beta_{4th}$ –Pro14 in  $\beta_{5th}$  and Gln19 in  $\beta_{4th}$ –Leu15 in  $\beta_{5th}$  on the cytoplasmic side, as well as Trp48 in  $\beta_{4th}$ –Pro53 in  $\beta_{5th}$  on the periplasmic side. Overall, the relative positioning of LH subunits in the complex may be partially maintained by these hydrogen bonds.

The interactions between the CaRC and its associated LH subunits are crucial for the formation of a stable CaRC-LH photocomplex (Figure 3B). On the periplasmic side, the crescent-shaped LH forms four hydrogen bond interactions with the M subunit, as well as one hydrogen bond interaction with the L subunit. These interactions involve specific residue pairs, including Ser31 in  $\alpha_{4th}$ -Asn70 in M, Ser31 in  $\alpha_{4th}\!\!-\!\!Asn72$  in M, Ser31 in  $\alpha_{5th}\!\!-\!\!Tyr71$  in M, Ser31 in  $\alpha_{7\text{th}}$ -Ser95 in M, and Ser31 in  $\alpha_{3\text{rd}}$ -Pro306 in L. The Ser31 residue in the LH  $\alpha$  apoprotein thus clearly plays a crucial role in the interaction with the central CaRC. On the cytoplasmic side, there is no interaction between LH and M or L subunits, but two hydrogen bonds (Ser5 in  $\alpha_{1st}$ -Gln10 in Cyt c and Ser32 in  $\alpha_{1st}$ -Thr38 in Cyt c) are present between the LH  $\alpha_{1st}$ apoprotein and the N-terminal TM helix of the Cyt c subunit (Figure 3C).

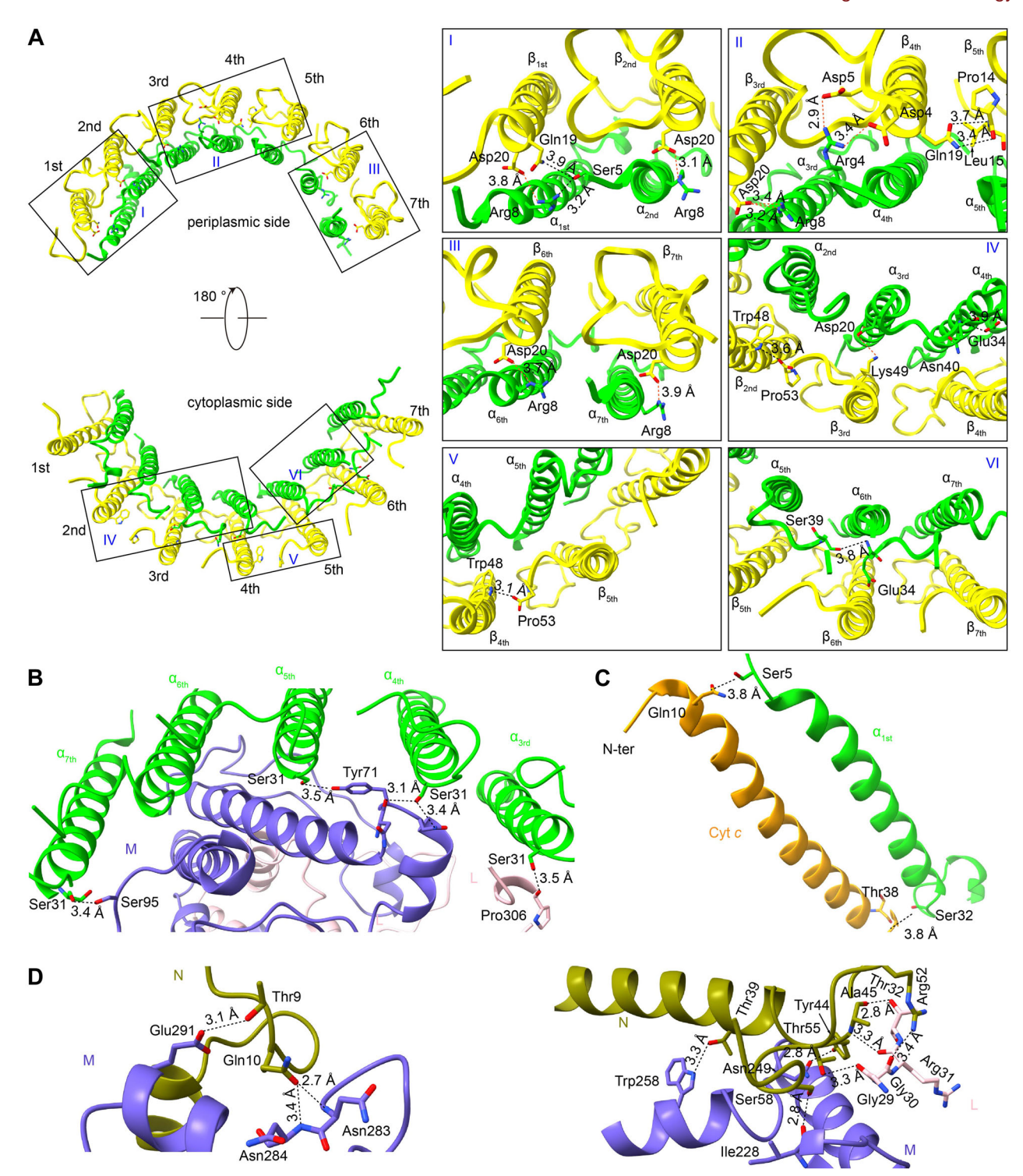


Figure 3. Interactions between subunits in the CaRC-LH complex

(A) Interaction network within the light-harvesting (LH) subunit and between adjacent LH subunits. (B) Interactions between LH antenna and CaRC. (C) Interactions between the N terminus of Cyt c and the  $\alpha$  apoprotein of LH<sub>1st</sub>. (D) Interactions between proteins N and L or the M subunit. All hydrogen bonds and salt bridges are indicated as black and red dashed lines, respectively.

In the CaRC-LH complex, the protein N adjacent to the L/M heterodimer is composed of a long central TM helix (from Pro17 to Ile41) and two short terminal flexible tails. The central TM helix of protein N binds to the CaRC

mainly through hydrophobic interactions with the M subunit. On the periplasmic surface, the N-terminal tail of the protein N is exposed to the membrane and is stabilized by hydrogen bond interactions with the M subunit. The and-conditions) on Wiley Online Library for rules of use; OA articles are governed by the applicable Creative Common:

#### Journal of Integrative Plant Biology

Structure of RC with seven LHs from Chloroflexus aurantiacus

C-terminal tail of protein N is located on the cytoplasmic side, where it forms hydrogen bonds with the L and M subunits (Figure 3D).

In Cfx. aurantiacus, the CaRC is associated with a very large chlorosome consisting of thousands of BChl molecules on the cytoplasmic side, which may largely compensate for the smaller light-harvesting area caused by the minimal number of LH subunits present in the CaRC-LH complex of this species. The surface potential of the CaRC-LH photocomplex on the cytoplasmic side may therefore contribute to the binding between the CaRC-LH complex and the chlorosome. Moreover, the surface potential of the CaRC-LH photocomplex on the cytoplasmic side is very different from that of RcRC-LH (Figure S9). First, each LH subunit in CaRC-LH contains more negatively charged Asp residues (Asp4, Asp5, and Asp6) than RcRC-LH on the lower part of the crescent-shaped LH formed by the N terminus of the outer β apoprotein. Second, CaRC features a long flexible region at the N terminus of the L subunit, which contains multiple positively charged amino acid residues (Lys5, Lys7, Arg10, Arg23, Arg26, and Arg31) and interacts with the surface of the M subunit, stabilizing the L/M heterodimer and increasing the positive charge on the surface of CaRC. Third, a negatively charged Asp12 residue in the RcRC is located in the  $\beta$  apoprotein, while the equivalent position in CaRC–LH is occupied by a positively charged Lys11 residue, creating a semicircle of non-continuous positive charges on the outer side of the LH antenna. Additionally, the C terminus of protein N, which is richer in positively charged amino acid residues (Arg47, Arg49, Arg52, Lys53, and Lys61) than protein Z of RcRC–LH (Arg51 and Lys56), further enhances the electropositivity on the surface of the CaRC–LH photocomplex facing the chlorosome. All of these characteristics may allow the CaRC–LH photocomplex to bind to the baseplate of chlorosome.

#### Menaquinone shuttling and ET pathways

In the CaRC-LH complex,  $Q_A$  and  $Q_B$  function as the primary and secondary acceptors for menaquinones, respectively (Kimura et al., 2023), a similar arrangement to that observed in RcRC-LH. In RcRC-LH, menaquinone molecules can shuttle freely through the space between the L/M heterodimer and

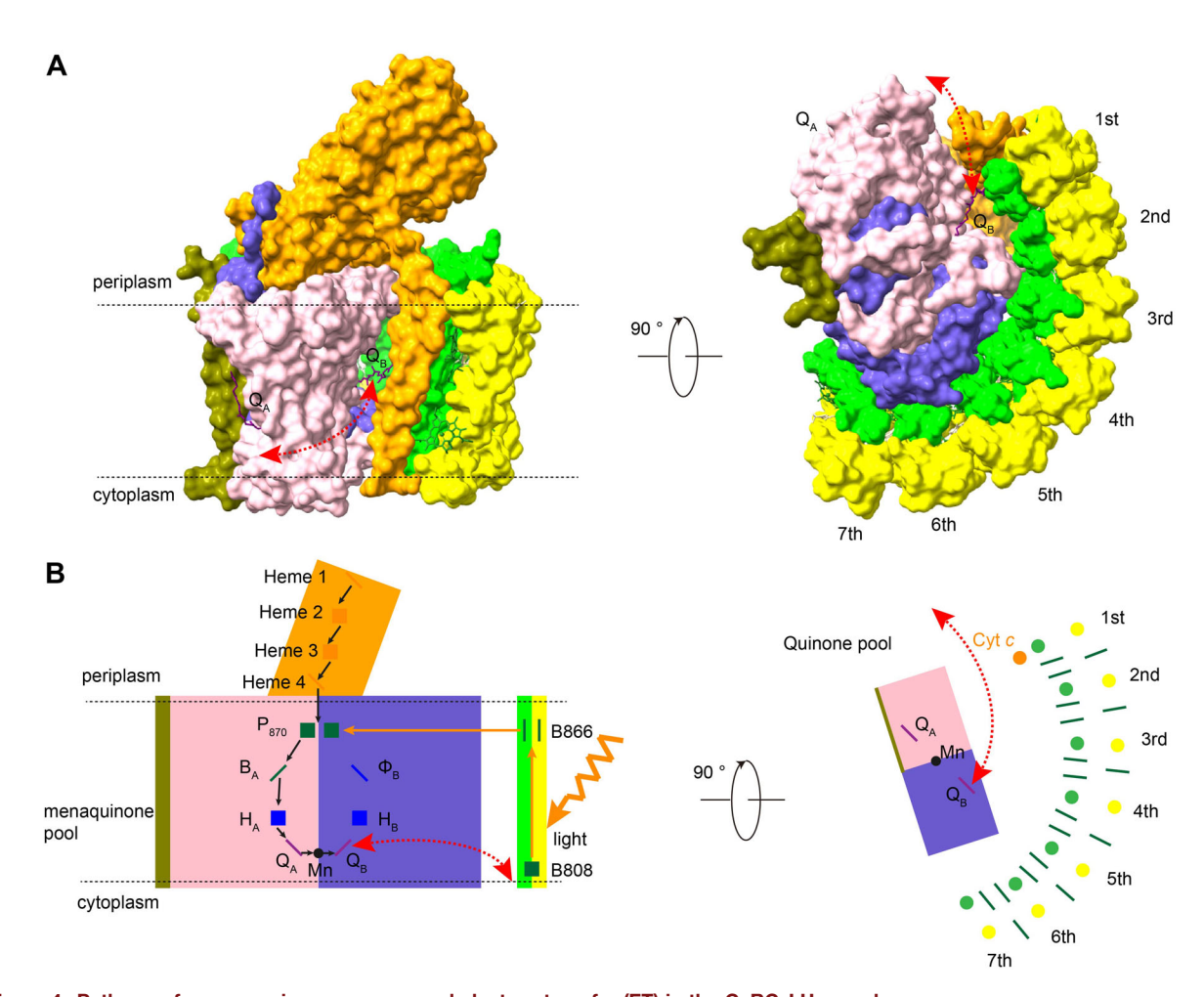


Figure 4. Pathways for menaquinone, energy, and electron transfer (ET) in the CaRC-LH complex (A) Side (left) and bottom-up (right) views of the proposed menaguinone channel of the CaRC-LH complex. (I

(A) Side (left) and bottom-up (right) views of the proposed menaquinone channel of the CaRC-LH complex. (B) Diagram of the energy, electron, and menaquinone transfer in the CaRC-LH complex. The direct shuttling of menaquinone between the menaquinone pool and  $Q_B$  is indicated by red dashed arrows. Pathways for energy and ET are represented by orange and black solid arrows, respectively.

LH<sub>1st-6th</sub>, eventually passing through an opening in the LH ring adjacent to the Q<sub>B</sub> site (Xin et al., 2018). Similarly, in CaRC-LH, ET predominantly occurs along the A branch of cofactors (Kirmaier and Holten, 1987; Wei et al., 2022). As shown in Figure 4, electrons travel sequentially from P<sub>870</sub> to B<sub>A</sub> and H<sub>A</sub>, then to Q<sub>A</sub>, before transferring through Mn to Q<sub>B</sub>. The reduced Q<sub>B</sub> then enters the menaguinone pool through a potential internal menaquinone channel. However, the absence of proteins X and Y in CaRC-LH compared with RcRC-LH results in a more open state that may facilitate menaguinone shuttling in CaRC-LH. Further experimental work will be needed to test this model and explore the potential physiological advantages of this distinctive CaRC-LH complex.

# **DISCUSSION**

Due to the intimate phylogenetic connection between their respective originating phototrophic bacteria, the RcRC-LH complex has frequently been employed as a substitute for the CaRC-LH complex (Collins et al., 2011; Xin et al., 2012). Our research revealed significant structural distinctions between the RC-LH complexes of these two closely related species, highlighting the remarkable diversity that can exist in this crucial component of the photosynthetic apparatus. In contrast with the structure of RcRC-LH, the CaRC-LH complex lacks proteins X, Y, and Z as well as eight LH subunits. Instead, it has one protein N in the position corresponding to protein Z in the RcRC, and only seven neighboring LH subunits surrounding the CaRC.

Furthermore, the fact that only seven LH subunits bind around the CaRC can also explain why Cfx. aurantiacus requires additional binding to the chlorosomes as a light-harvesting antenna. In fact, phylum Chloroflexi currently harbors at least three typical photosynthetic apparatuses (Figure S10). Candidatus Chlorohelix allophototropha, a chlorosome-containing phototroph, contains a Fenna-Matthews-Olson (FMO) complex that transfers energy from the chlorosome to its Type I RC. Cfx. aurantiacus J-10-fl, another chlorosome-containing phototroph, only possesses a crescent-shaped LH antenna complex whose chlorosomes interface with its Type II RC directly. Finally, Rfl. castenholzii has no FMO or chlorosome, only possessing an open elliptical LH ring that surrounds its Type II RC. In terms of evolution, photosynthetic organisms containing chlorosomes are believed to be more ancient (Xin et al., 2018). Therefore, we speculate that both Candidatus Chlorohelix allophototropha and Cfx. aurantiacus J-10-fl are older than Rfl. castenholzii.

In purple bacteria, the RC-bound Cyt c subunits are categorized into two groups depending on the presence or absence of a signal peptide followed by a cysteine (Cys) residue at the N terminus (Tani et al., 2022a). In Cyt c subunits containing the signal peptide and Cys residue, Cyt c is truncated at the N-terminal Cys residue, has no TM domain, and is anchored to the surface of the RC on the periplasmic side by covalently bound lipids; these are found in species including Tch. tepidum (Yu et al., 2018), Blc. viridis (Qian et al., 2018),

Thiorhodovibrio strain 970 (Tani et al., 2020), and A. tepidum (Tani et al., 2022b). In the other group, Cyt c subunits lack this Cys residue and have the full N terminus inserted into the membrane; this structure has been proposed to be more ancient than the lipid-anchored form (Liu et al., 2023) and is found in species such as Rpi. globiformis (Tani et al., 2022a). The CaRC-LH structure revealed a Cys-lacking Cyt c subunit, and another previously reported FAP in phylum Chloroflexi, Rfl. castenholzii, also has a Cyt c subunit lacking this Cys residue. Thus, at least two kinds of FAPs in phylum Chloroflexi possess Cyt c subunits lacking the Cys residue, although it is not clear whether phylum Chloroflexi also includes species with the Cyt c subunit containing the Cys residue.

To better elucidate the interaction patterns within the unique CaRC-LH complex, we analyzed the interactions of protein N with CaRC, the interactions within individual LH  $\alpha\beta$ -heterodimers and between neighboring LH subunits, and the interplay between the crescent-shaped LH and the CaRC. In addition to significant hydrophobic interactions, there are also hydrogen bond interactions between protein N and the CaRC and between LH and the CaRC, as well as between adjacent LH subunits. Within individual LH subunits, besides hydrogen bond interactions, there are also partial salt bridge interactions. All these unique interactions contribute to the relative stability of the CaRC-LH complex, which consists of only seven LH subunits. Based on the current 2D averages or 3D maps, we did not observe the CaRC complex surrounded by an elliptical LH ring, contrary to previous reports (Bína et al., 2014). Despite efforts to reduce the concentration of n-dodecyl-β-D-maltoside (β-DDM) detergent from 1.5% (w/v) to 1.0% (w/v) and eventually to 0.5% (w/v), this structure was not resolved. Moreover, when visualizing the CaRC-LH complex in its native environment using atomic force microscopy (AFM), we also did not find an elliptical LH structure. If such an LH ring exists in CaRC-LH, the unobserved portion of the LH ring must interact more weakly with the CaRC, making it more easily dissociated; this is in contrast with the half-ring observed in the RcRC-LH complex. Thus, we speculate that Cfx. aurantiacus may dynamically adjust its light-harvesting capability by assembling either a full circle or half circle antenna in response to the changes of environment. Furthermore, a puzzle still exists as to why the ET rate in CaRC is slower than in RcRC, which may require further experiments to elucidate.

In summary, we present a comprehensive analysis of the composition, structural characteristics, and key interaction forces that contribute to the stability of the minimal RC-LH complex from Cfx. aurantiacus. Notably, its distinctive structure, with only seven LH subunits, allows us to propose the possible route for quinone shuttling within the photocomplex and offer a plausible explanation for the CaRC-LH complex's binding to the chlorosome. Our findings provide valuable insight into the structural variability of photocomplexes within the Chloroflexi phylum, shedding light on their critical role in enabling photosynthesis in phototrophic bacteria that adapt to diverse environmental conditions.

# **MATERIALS AND METHODS**

#### Purification of the CaRC-LH

Cfx. aurantiacus cells (DSM 635, Leibniz Institute DSMZ-German Collection of Microorganisms and Cell Cultures) were cultivated in 0.9 L of Chloroflexus medium (He et al., 2015) at 50°C for 2 weeks, with a light intensity of ~2.000 lx. as described previously with some modifications (Pierson and Thornber, 1983). All of the following steps were performed under a green light. The cells were collected by centrifugation at 8,000 g for 16 min at 4°C. The resulting pellet, weighing 5 g (wet weight), was suspended in 10 mL of lysis buffer (20 mM Tris-HCl, pH 7.6). The cells were lysed under 2,000 bar pressure with a low-temperature ultra-highpressure cell crusher (JNBIO) and centrifuged at 4°C, 8,000 g for 10 min to remove cell debris and unbroken cells. The supernatant was centrifuged at 46,200 g for 90 min, and the resulting pellet containing membranes was solubilized in 1% (w/v) β-DDM in an ice bath for 70 min. The insoluble component was removed by centrifugation at 4°C, 57,750 g for 60 min, and the supernatant containing the CaRC-LH was collected and further purified by ultracentrifugation of a linear sucrose gradient (from 300 to 900 mM) at 243,500 g for 16 h at 4°C, yielding three bands in the gradient (Figure S1A). Of these three bands (B1-B3), B1 contained free pigments, B2 contained the CaRC component, and B3 mainly contained the CaRC-LH sample. The major polypeptides (L, M, Cyt c, protein N and LH-β) in B3 were identified using sodium dodecyl sulfate-polyacrylamide gel electrophoresis (SDS-PAGE) and mass spectrometry (Figure S1B, C). The absorption spectrum obtained at room temperature showed two peaks in the Q<sub>Y</sub> band region, one at 812 nm and another at 864 nm (Figure S1D). The B3 sample was eventually concentrated with Amicon ultra 100 K filters (Millipore, USA) and equilibrated with lysis buffer to 20 mg/mL to be used for subsequent experiments.

## Cryo-EM sample preparation and data collection

Here, 4 µL of the CaRC-LH protein sample, at a concentration of 3.99 mg/mL, was loaded onto the holey carbon grids (Quantifoil Au grid, 400 mesh, R1.2/1.3) and rapidly plungefrozen into liquid ethane pre-cooled with liquid nitrogen using a Vitrobot Mark IV (FEI). The plunge-freezing process was conducted under the following conditions: a waiting time of 10 s, blotting force set to −1, blotting time of 4 s, and a chamber environment maintained at 100% humidity and 8°C. The quality of cryo-EM grids was evaluated using either an FEI Tecnai Arctica TEM D683 or an FEI Talos Arctica TEM 9950610 at 200 kV. High-quality grids were used for imaging on an FEI Titan Krios TEM D3786 operated at 300 kV. The Titan Krios was equipped with a K3 Summit direct electron detector (Gatan) and a GIF Quantum energy filter (Gatan) with the slit width set to 20 eV. Automatic data collection was performed using AutoEMation software (Lei and Frank, 2005) in super-resolution mode, with defocus values ranging from -1.0 to  $-1.5 \,\mu m$  and a nominal magnification of  $\times 105,000$ , corresponding to a pixel size of 0.42165 Å. Each movie stack was fractionated into 32 frames with a total dose of  $50.2\,\mathrm{e}^{-}/\mathrm{Å}^{2}$ , and 5.757 movie stacks were recorded.

#### Cryo-EM image processing

The movie stacks were motion-corrected with MotionCor2 (Zheng et al., 2017), binned to a pixel size of 0.8433 Å, and all motion-corrected images were further processed using cryoSPARC (Figure S2C) (Punjani et al., 2017). Contrast transfer function (CTF) parameters were determined by patch CTF estimation in cryoSPARC. After the removal of micrographs with a CTF fit resolution worse than 5 Å, 5,697 micrographs were retained. From these, 4,373,000 particles were autopicked from 5.697 micrographs using a blob picker (particle diameters from 50 to 400 Å) and subjected to 2D classification. After several rounds of screening for 2D classification, it was seen from 2D averages that the sample was clearly a mixture of several protein complexes. Ab initio reconstruction (five classes) was first attempted to isolate different protein structures from the 3D data, but no 3D structure was obtained for CaRC-LH, which may have been due to the low ratio and low molecular mass or signal-tonoise ratio of CaRC-LH compared with other protein complexes mixed in the sample. Therefore, particles that obviously did not belong to CaRC-LH were excluded from the 2D averages, retaining 90,033 particles for another round of ab initio reconstruction (three classes). A good initial structure of CaRC-LH with 38,324 particles was selected for non-uniform refinement (Punjani et al., 2020) and local refinement; however, only a moderate-resolution structure of 4.6 Å was reconstructed, which may have been due to a small number of particles and/or a mixture of some bad particles. These 38,324 particles were used as the training dataset for Topaz (Bepler et al., 2019), which was applied for picking a larger number and more accurate set of CaRC-LH particles, resulting in 589,857 particles picked from 5,686 micrographs. Several rounds of 2D classification were performed again to remove junk particles and other protein particles. After this step, 74,517 particles were selected for ab initio reconstruction (three classes), and a good CaRC-LH initial structure was generated with 36,181 particles. Upon further processing of this structure with non-uniform refinement, local CTF refinement, and local refinement, a 3.05-Å resolution map was obtained. To improve the quality and interpretability of the EM map, the final map was sharpened using EMReady (He et al., 2023). The map sharpened by EMReady was used for figure preparation and initial model building, while the raw sharpened map was used for model refinement. Resolution values were estimated using the gold-standard Fourier shell correlation (GSFSC) method in cryoSPARC and using 3DFSC (Tan et al., 2017).

# Modeling and refinement

The atomic model of the CaRC-LH complex was initially auto-built using CryoNet (https://cryonet.ai/build/) (Xu et al., 2019) by providing the cryo-EM structure and the known

protein sequences of the CaRC-LH. LH-α precisely matched the specific amino acid side chains with the EM density (Figure S3), although the sequence for LH- $\alpha$  was not tested by mass spectrometry. The determination of the cofactors was primarily based on previous HPLC analysis results (Xin et al., 2005). The initial positions and orientations of these cofactors were derived from the atomic model of the RC-LH complex from Roseiflexus castenholzii (PDB code: 8HJU) by docking the 8HJU model into the cryo-EM map of CaRC-LH using UCSF ChimeraX (Pettersen et al., 2021). Subsequently, the accurate coordinates and orientations of the residue side chains and the cofactors were manually adjusted and optimized based on the EM density using Coot (Emsley et al., 2010) and further refined by real-space refinement in PHENIX (Adams et al., 2010). The statistics for data processing and structure refinement are summarized in Table S1.

### **Data availability statement**

The atomic coordinates and EM maps for the CaRC-LH complex have been deposited in the Protein Data Bank (www.rcsb.org) and Electron Microscopy Data Bank (www. ebi.ac.uk/pdbe/emdb/) under accession code 8YDM for the atomic model, EMD-39177 for the raw sharpened map, and EMD-62657 for the EMReady-sharpened map, respectively. The data that support this study are available from the corresponding author upon request. All data needed to evaluate the conclusions in the paper are present in the paper and/or the Supplemental Information.

# **ACKNOWLEDGEMENTS**

We thank Jianlin Lei and the staff at the Tsinghua University Branch of the National Center for Protein Sciences, Beijing, for providing facility support, and the "Explorer 100" cluster system of the Tsinghua National Laboratory for Information Science and Technology for providing computation resources. This project was funded by the National Natural Science Foundation of China (32270260, 32070267, 32200206, 32241030, and 32271245), the Taishan Scholars Project (tsqn20240516), and the Shandong Provincial Natural Science Foundation, China (ZR2019ZD48 and ZR2020QC057).

# **CONFLICTS OF INTEREST**

The authors declare no competing interests.

## **AUTHOR CONTRIBUTIONS**

X.Q., S.-F.S., and S.D. conceived and designed the research. S.D., G.H., and X.Q. drafted the manuscript. G.H. processed the cryo-EM data, built and refined the structure model and analyzed the data. L.M. prepared the sample, L.L. and J.J. assisted in sample preparation. M.-J.W. and J.-P.Z. carried out AFM analysis. S.D., X.Q., and G.H. revised the manuscript. All authors read and approved of its content.

Edited by: Jiamu Du, Southern University of Science and Technology,

Received Jun. 5, 2024; Accepted Jan. 10, 2025

## REFERENCES

- Adams, P.D., Afonine, P.V., Bunkoczi, G., Chen, V.B., Davis, I.W., Echols, N., Headd, J.J., Hung, L.W., Kapral, G.J., Grosse-Kunstleve, R.W., et al. (2010). PHENIX: A comprehensive Python-based system for macromolecular structure solution. Acta Crystallogr. D. Biol. Crystallogr. 66: 213-221.
- Becker, M., Nagarajan, V., Middendorf, D., Parson, W.W., Martin, J.E., and Blankenship, R.E. (1991). Temperature dependence of the initial electron-transfer kinetics in photosynthetic reaction centers of Chloroflexus aurantiacus. Biochim. Biophys. Acta 1057: 299-312.
- Bepler, T., Morin, A., Rapp, M., Brasch, J., Shapiro, L., Noble, A.J., and Berger, B. (2019). Positive-unlabeled convolutional neural networks for particle picking in cryo-electron micrographs. Nat. Methods 16:
- Bína, D., Gardian, Z., Vácha, F., and Litvín, R. (2014). Supramolecular organization of photosynthetic membrane proteins in the chlorosomecontaining bacterium. Photosynth. Res. 122: 13-21.
- Blankenship, R.E. (2014). Molecular Mechanisms of Photosynthesis. Wiley Blackwell, Chichester UK. pp. 59-84.
- Bracun, L., Yamagata, A., Christianson, B.M., Shirouzu, M., and Liu, L.N. (2023). Cryo-EM structure of a monomeric RC-LH1-PufX supercomplex with high-carotenoid content from Rhodobacter capsulatus. Structure 31: 318-328.
- Bracun, L., Yamagata, A., Christianson, B. M., Terada, T., Canniffe, D. P., Shirouzu, M., and Liu, L.-N. (2021). Cryo-EM structure of the photosynthetic RC-LH1-PufX supercomplex at 2.8-Å resolution. Sci. Adv. 7: eabf8.
- Cao, P., Bracun, L., Yamagata, A., Christianson, B.M., Negami, T., Zou, B., Terada, T., Canniffe, D.P., Shirouzu, M., Li, M., et al. (2022). Structural basis for the assembly and quinone transport mechanisms of the dimeric photosynthetic RC-LH1 supercomplex. Nat. Commun. 13: 1977.
- Chen, J.H., Wu, H., Xu, C., Liu, X.C., Huang, Z., Chang, S., Wang, W., Han, G., Kuang, T., Shen, J.R., et al. (2020). Architecture of the photosynthetic complex from a green sulfur bacterium. Science 370: eabb6350.
- Collins, A.M., Kirmaier, C., Holten, D., and Blankenship, R.E. (2011). Kinetics and energetics of electron transfer in reaction centers of the photosynthetic bacterium Roseiflexus castenholzii. Biochim. Biophys. Acta 1807: 262-269.
- Dong, S.S., Huang, G.Q., Wang, C.H., Wang, J.J., Sui, S.F., and Qin, X.C. (2022). Structure of the Acidobacteria homodimeric reaction center bound with cytochrome c. Nat. Commun. 13: 7745.
- Emsley, P., Lohkamp, B., Scott, W.G., and Cowtan, K. (2010). Features and development of Coot. Acta Crystallogr. D Biol. Crystallogr. 66: 486-501.
- Gisriel, C., Sarrou, I., Ferlez, B., Golbeck, J.H., Redding, K.E., and Fromme, R. (2017). Structure of a symmetric photosynthetic reaction center-photosystem. Science 357: 1021-1025.
- Hager-Braun, C., Xie, D.L., Jarosch, U., Herold, E., Buttner, M., Zimmermann, R., Deutzmann, R., Hauska, G., and Nelson, N. (1995). Stable photobleaching of P840 in Chlorobium reaction center preparations: Presence of the 42-kDa bacteriochlorophyll a protein and a 17-kDa polypeptide. Biochemistry 34: 9617-9624.

- Hanada, S., Takaichi, S., Matsuura, K., and Nakamura, K. (2002).
  Roseiflexus castenholzii gen. nov., sp. nov., a thermophilic, filamentous, photosynthetic bacterium that lacks chlorosomes. Int. J. Syst. Evol. Microbiol. 52: 187–193.
- He, J., Li, T., and Huang, S.Y. (2023). Improvement of cryo-EM maps by simultaneous local and non-local deep learning. Nat. Commun. 14: 3217.
- He, L., Wang, Y., You, L., Khin, Y., Tang, J.K., and Tang, Y.J. (2015). Glycine cleavage powers photoheterotrophic growth of *Chloroflexus aurantiacus* in the absence of H2. Front. Microbiol. **6:** 1467.
- Jun, D., Richardson-Sanchez, T., Mahey, A., Murphy, M.E.P., Fernandez, R.C., and Beatty, J.T. (2020). Introduction of the menaquinone biosynthetic pathway into and synthesis of menaquinone for incorporation into heterologously expressed integral membrane proteins. ACS Synth. Biol. 9: 1190–1200.
- Kimura, Y., Tani, K., Madigan, M.T., and Wang-Otomo, Z.Y. (2023).
  Advances in the spectroscopic and structural characterization of core light-harvesting complexes from purple phototrophic. Bacteria. J. Phys. Chem. B. 127: 6–17.
- Kirmaier, C., Blankenship, R. E., and Holten, D. (1986). Formation and decay of radical-pair state P<sup>+</sup>I- in *Chloroflexus aurantiacus* reaction centers. Biochim. Biophys. Acta 850: 275–285.
- Kirmaier, C., and Holten, D. (1987). Primary photochemistry of reaction centers from the photosynthetic purple bacteria. Photosynth. Res. 13: 225–260.
- Lei, J., and Frank, J. (2005). Automated acquisition of cryo-electron micrographs for single particle reconstruction on an FEI Tecnai electron microscope. J. Struct. Biol. 150: 69–80.
- Liu, L.N., Bracun, L., and Li, M. (2023). Structural diversity and modularity of photosynthetic RC-LH1 complexes. Trends Microbiol. 32: 38–52.
- Pedersen, M.O., Linnanto, J., Frigaard, N.U., Nielsen, N.C., and Miller, M. (2010). A model of the protein-pigment baseplate complex in chlorosomes of photosynthetic green bacteria. Photosynth. Res. 104: 233–243.
- Pettersen, E.F., Goddard, T.D., Huang, C.C., Meng, E.C., Couch, G.S., Croll, T.I., Morris, J.H., and Ferrin, T.E. (2021). UCSF ChimeraX: Structure visualization for researchers, educators, and developers. Protein Sci. 30: 70–82.
- Pierson, B.K., and Castenholz, R.W. (1974). A phototrophic gliding filamentous bacterium of hot springs, *Chloroflexus aurantiacus*, gen. and sp. nov. Arch. Microbiol. **100:** 5–24.
- Pierson, B.K., and Thornber, J.P. (1983). Isolation and spectral characterization of photochemical reaction centers from the thermophilic green bacterium *Chloroflexus aurantiacus* strain J-10-f1. Proc. Natl. Acad. Sci. U.S.A. 80: 80–84.
- Punjani, A., Rubinstein, J.L., Fleet, D.J., and Brubaker, M.A. (2017). cryoSPARC: Algorithms for rapid unsupervised cryo-EM structure determination. Nat. Methods 14: 290–296.
- Punjani, A., Zhang, H., and Fleet, D.J. (2020). Non-uniform refinement: Adaptive regularization improves single-particle cryo-EM reconstruction. Nat. Methods 17: 1214–1221.
- Qi, C.H., Wang, G.L., Wang, F.F., Xin, Y., Zou, M.J., Madigan, M.T., Wang-Otomo, Z.Y., Ma, F., and Yu, L.J. (2023). New insights on the photocomplex of *Roseiflexus castenholzii* revealed from comparisons of native and carotenoid-depleted complexes. J. Biol. Chem. 299: 105057.
- Qian, P., Croll, T.I., Hitchcock, A., Jackson, P.J., Salisbury, J.H., Castro-Hartmann, P., Sader, K., Swainsbury, D.J.K., and Hunter, C.N. (2021a). Cryo-EM structure of the dimeric RC-LH1 core complex at 2.9 A: The structural basis for dimerisation. Biochem. J. 478: 3923-3937
- Qian, P., Gardiner, A.T., Simova, I., Naydenova, K., Croll, T.I., Jackson, P.J., Nupur, Kloz, M., Cubakova, P., Kuzma, M., et al. (2022). 2.4-Å

- structure of the double-ring Gemmatimonas phototrophica photosystem. Sci. Adv. 8: eabk3139.
- Qian, P., Siebert, C.A., Wang, P.Y., Canniffe, D.P., and Hunter, C.N. (2018). Cryo-EM structure of the *Blastochloris viridis* LH1-RC complex at 2.9 Å. Nature **556**: 203–208.
- Qian, P., Swainsbury, D.J.K., Croll, T.I., Salisbury, J.H., Martin, E.C., Jackson, P.J., Hitchcock, A., Castro-Hartmann, P., Sader, K., and Hunter, C.N. (2021b). Cryo-EM structure of the monomeric *Rhodobacter sphaeroides* RC-LH1 core complex at 2.5 Å. Biochem. J. 478: 3775–3790.
- Rosenberg, E. (2014). The Prokaryotes: Other Major Lineages of Bacteria and the Archaea. Springer, New York. pp. 515–529.
- Saer, R.G., and Blankenship, R.E. (2017). Light harvesting in phototrophic bacteria: Structure and function. Biochem. J. 474: 2107–2131.
- Swainsbury, D.J.K., Qian, P., Hitchcock, A., and Hunter, C.N. (2023). The structure and assembly of reaction centre-light-harvesting 1 complexes in photosynthetic bacteria. Biosci. Rep. 43: BSR20220089.
- Swainsbury, D.J.K., Qian, P., Jackson, P.J., Faries, K.M., Niedzwiedzki, D.M., Martin, E.C., Farmer, D.A., Malone, L.A., Thompson, R.F., Ranson, N.A., et al. (2021). Structures of *Rhodopseudomonas palustris* RC-LH1 complexes with open or closed quinone channels. Sci. Adv. 7: eabe2631.
- Taisova, A.S., Keppen, O.I., Lukashev, E.P., Arutyunyan, A.M., and Fetisova, Z.G. (2002). Study of the chlorosomal antenna of the green mesophilic filamentous bacterium *Oscillochloris trichoides*. Photosynth. Res. 74: 73–85.
- Tan, Y.Z., Baldwin, P.R., Davis, J.H., Williamson, J.R., Potter, C.S., Carragher, B., and Lyumkis, D. (2017). Addressing preferred specimen orientation in single-particle cryo-EM through tilting. Nat. Methods 14: 793–796.
- Tang, K.H., Barry, K., Chertkov, O., Dalin, E., Han, C.S., Hauser, L.J., Honchak, B.M., Karbach, L.E., Land, M.L., Lapidus, A., et al. (2011). Complete genome sequence of the filamentous anoxygenic phototrophic bacterium *Chloroflexus aurantiacus*. BMC Genomics 12: 334.
- Tani, K., Kanno, R., Ji, X.C., Hall, M., Yu, L.J., Kimura, Y., Madigan, M.T., Mizoguchi, A., Humbel, B.M., and Wang-Otomo, Z.Y. (2021a).
  Cryo-EM structure of the photosynthetic LH1-RC complex from *Rhodospirillum rubrum*. Biochemistry **60**: 2483–2491.
- Tani, K., Kanno, R., Ji, X.C., Satoh, I., Kobayashi, Y., Hall, M., Yu, L.J., Kimura, Y., Mizoguchi, A., Humbel, B.M., et al. (2023). Rhodobacter capsulatus forms a compact crescent-shaped LH1-RC photocomplex. Nat. Commun. 14: 846.
- Tani, K., Kanno, R., Kurosawa, K., Takaichi, S., Nagashima, K.V.P., Hall, M., Yu, L.J., Kimura, Y., Madigan, M.T., Mizoguchi, A., et al. (2022a). An LH1-RC photocomplex from an extremophilic phototroph provides insight into origins of two photosynthesis proteins. Commun. Biol. 5: 1197.
- Tani, K., Kanno, R., Makino, Y., Hall, M., Takenouchi, M., Imanishi, M., Yu, L.J., Overmann, J., Madigan, M.T., Kimura, Y., et al. (2020). Cryo-EM structure of a  $Ca(^{2+})$ -bound photosynthetic LH1-RC complex containing multiple  $\alpha\beta$ -polypeptides. Nat. Commun. 11: 4955.
- Tani, K., Kobayashi, K., Hosogi, N., Ji, X.C., Nagashima, S., Nagashima, K.V.P., Izumida, A., Inoue, K., Tsukatani, Y., Kanno, R., et al. (2022b). A Ca(<sup>2+</sup>)-binding motif underlies the unusual properties of certain photosynthetic bacterial core light-harvesting complexes. J. Biol. Chem. 298: 101967.
- Tani, K., Nagashima, K.V.P., Kanno, R., Kawamura, S., Kikuchi, R., Hall, M., Yu, L.J., Kimura, Y., Madigan, M.T., Mizoguchi, A., et al. (2021b). A previously unrecognized membrane protein in the *Rho-dobacter sphaeroides* LH1-RC photocomplex. Nat. Commun. 12: 6300.

17447909, O, Downloaded from https://onlinelibrary.wiley.com/doi/10.1111/jipb.13853 by Tsinghua University Library, Wiley Online Library on [17/02/2025]. See the Terms and-conditions) on Wiley Online Library for rules of use; OA are governed by the applicable Creative Commo

- Tsuji, J.M., Shaw, N.A., Nagashima, S., Venkiteswaran, J.J., Schiff, S.L., Watanabe, T., Fukui, M., Hanada, S., Tank, M., and Neufeld, J.D. (2024). Anoxygenic phototroph of the Chloroflexota uses a type I reaction centre. Nature 627: 915-922.
- Vasmel, H., Van Dorssen, R.J., De Vos, G.J., and Amesz, J. (1986). Pigment organization and energy transfer in the green photosynthetic bacterium Chloroflexus aurantiacus: I. The cytoplasmic membrane. Photosynth. Res. 7: 281-294.
- Ward, L.M., Cardona, T., and Holland-Moritz, H. (2019). Evolutionary implications of anoxygenic phototrophy in the bacterial phylum Candidatus Eremiobacterota (WPS-2). Front. Microbiol. 10: 1658.
- Wei, R.J., Zhang, Y.Y., Mao, J.J., Kaur, D., Khaniya, U., and Gunner, M.R. (2022). Comparison of proton transfer paths to the Q and Q sites of the photosynthetic reaction centers. Photosynth. Res. 152: 153-165.
- Xin, J., Shi, Y., Zhang, X., Yuan, X., Xin, Y., He, H., Shen, J., Blankenship, R.E., and Xu, X. (2023). Carotenoid assembly regulates guinone diffusion and the Roseiflexus castenholzii reaction center-light harvesting complex architecture, eLife 12: e88951.
- Xin, Y., Lin, S., and Blankenship, R.E. (2007). Femtosecond spectroscopy of the primary charge separation in reaction centers of Chloroflexus aurantiacus with selective excitation in the Q<sub>Y</sub> and Soret bands. J. Phys. Chem. A 111: 9367–9373.
- Xin, Y., Lin, S., Montano, G.A., and Blankenship, R.E. (2005). Purification and characterization of the B808-866 light-harvesting complex from green filamentous bacterium Chloroflexus aurantiacus. Photosynth. Res 86: 155-163
- Xin, Y., Pan, J., Collins, A.M., Lin, S., and Blankenship, R.E. (2012). Excitation energy transfer and trapping dynamics in the core complex of the filamentous photosynthetic bacterium Roseiflexus castenholzii. Photosynth, Res. 111: 149-156.
- Xin, Y., Shi, Y., Niu, T., Wang, Q., Niu, W., Huang, X., Ding, W., Yang, L., Blankenship, R.E., Xu, X., et al. (2018). Crvo-EM structure of the RC-LH core complex from an early branching photosynthetic prokarvote. Nat. Commun. 9: 1568.
- Xu, K., Wang, Z., Shi, J.P., Li, H.S., and Zhang, Q.F.C. (2019). A2-Net\_ molecular structure estimation from Cryo-EM density volumes. AAAI 33: 1230-1237.

- Yu, L.J., Suga, M., Wang-Otomo, Z.Y., and Shen, J.R. (2018). Structure of photosynthetic LH1-RC supercomplex at 1.9 Å resolution. Nature **556:** 209-213
- Zheng, L., Zheng, Z.G., Li, X.Y., Wang, G.P., Zhang, K., Wei, P.J., Zhao, J.D., and Gao, N. (2021). Structural insight into the mechanism of energy transfer in cyanobacterial phycobilisomes. Nat. Commun.
- Zheng, S.Q., Palovcak, E., Armache, J.P., Verba, K.A., Cheng, Y., and Agard, D.A. (2017). MotionCor2: Anisotropic correction of beaminduced motion for improved cryo-electron microscopy. Nat. Methods 14: 331-332

## SUPPORTING INFORMATION

Additional Supporting Information may be found online in the supporting information tab for this article: http://onlinelibrary.wiley.com/doi/10.1111/ iipb.13853/suppinfo

Figure S1. Preparation and characterization of the CaRC-LH complex

Figure S2. Cryo-EM data and map quality of the CaRC complex

Figure S3. Representative cryo-EM maps of the subunits and cofactors in the CaRC complex

Figure S4. Comparison of the cofactor arrangements along the electron transfer (ET) chains in CaRC and RcRC

Figure S5. Comparison of protein N and NWG19514.1 from Cfx. aurantiacus and protein Z from Rfl. castenholzii

Figure S6. Comparison of the distribution of LH and LH1 from Cfx. aurantiacus and Rba. capsulatus, viewed from the plane of the membrane and from the cytoplasmic side

Figure S7. Sequence alignments of various LH- $\alpha$  or LH- $\beta$  apoprotein phototrophic bacteria

Figure S8. Shortest edge-to-edge distances between adjacent porphyrin rings in the CaRC-LH and RcRC-LH

Figure S9. Surface electrostatic potential of CaRC-LH and RcRC-LH (PDB ID: 8J5P)

Figure S10. Three typical photosynthetic apparatuses in phylum Chloro-

Table S1. Cryo-EM data collection, refinement, and validation statistics of the CaRC-LH complex



Scan the QR code to view JIPB on WeChat (WeChat: jipb1952)



Scan the QR code to view JIPB on Twitter (Twitter: @JIPBio)